BMC Chemistry

RESEARCH ARTICLE

Open Access

Spectral, thermal, antimicrobial studies for silver(I) complexes of pyrazolone derivatives

Soha F. Mohamed[1], Wesam S. Shehab[1], Aboubakr M. Abdullah[2*], Mostafa H. Sliem[2] and Walaa H. El-Shwiniy[1,3*]

Abstract

Background: Synthesize new complexes of Ag(I) to enhance efficacy or stability and also, pharmacological activities on the operation of pyrazolone's biological properties.

Results: Efficient and high yielding pathways starting from the versatile and readily available 3-methyl-1-phenyl-5-pyrazolone by Knoevenagel condensation of a sequence of 4-arylidene-3-methyl-1-phenyl-5-pyrazolone derivatives (**2a-c**) have been formed by the reaction of various substituted aromatic aldehydes Used as ligands to synthesize Ag(I) chelates. Synthesized compounds and their complexes have been characterized by elemental analysis, magnetic and spectroscopic methods (IR, ^{13}C, $^{1}HNMR$, mass) and thermal analysis. The spectrophotometric determinations suggest distorted octaedral geometry for all complexes. Both ligands and their metal complexes have also been tested for their antibacterial and antifungal efficacy.

Conclusions: Newly synthesized compounds have shown potent antimicrobial activity. The results showed that the complex 's high activity was higher than its free ligands, and that Ag(I)-L_3 had the highest activity.

Keywords: Pyrazolones, Ag(i) complexes, Knoevenagel condensation, Antimicrobial activity

Introduction

Pyrazolone chemistry began in 1883 when Ludwig Knorr first reacted to phenyl hydrazine with aceto-acetate ester. As pyrazolones were discovered as binding components for azo dyes in the late 1800s, they rapidly increased in importance. Today, pyrazolon is still an significant trade precursor to dyes and pharmaceuticals. Pyrazolone is a biologically important scaffold associated with different pharmacological activities such as antimicrobials [1–5], anti-inflammatory [6], analgesic [7], antidepressant [8], anticonvulsant [9], antidiabetic [10], antihyperlipidemic [11, 12], antiviral [13, 14], anti-tuberculosis [15, 16], antioxidant [17, 18] and anticancer [19, 20]. For several years, the preparation of pyrazolone and its derivatives has attracted significant attention from organic and medicinal chemists, as they belong to a class of compounds with promising results in medicinal chemistry. The heterocycles condensed to the pyrazole ring are an important source of bioactive molecules [21, 22]. Compounds containing both pyrazole and other essential heterocyclic active structural units usually demonstrate more remarkable biological activity. A number of condensed pyrazole derivatives have been reported as four-fold antibacterial agents against Gram-positive and Gram-negative bacteria compared to general pyrazole compounds [23, 24]. A digit of antimicrobial active silver(I) complexes have the capacity to disrupt microbial transpiration as well as block tyrosinase synthesis and are extremely cytotoxic to cancer cells [24]. Massive attention in silver ions (Ag(I)) as a broad spectrum antimicrobial has upped the size and importance of in vitro

*Correspondence: bakr@qu.edu.qa; abubakr_2@yahoo.com; whelmy@ub.edu.sa
[1] Department of Chemistry, Faculty of Science, Zagazig University, Zagazig 44519, Egypt
[2] Center for Advanced Materials, Qatar University, P.O. Box 2713, Doha, Qatar
Full list of author information is available at the end of the article

biocompatibility research [25]. Silver ions are toxic to many bacteria, viruses, algae and fungi. Silver-based medicines have been widely used for this task for decades [26]. The objective of this study is to display the synthesis and characterization of three Ag(I) pyrazolone complexes in an attempt to verify the mode of coordination and the biological properties of the final complexes.

Results and discussion

Synthesis and formulation

A sequence of derivatives of 4-arylidene-3-methyl-1-phenyl-5-pyrazolone (4-(4-dimethylamino benzylidene)-3-methyl-1-phenyl-1*H*-pyrazol-5(4*H*)-one (2a) L_1, 4-(4-Thiophene)-3-methyl-1-phenyl-1*H*pyrazol-5(4*H*)-one (2b) L_2, 4-(4-methoxy benzylidene)-3-methyl-1-phenyl-1*H*pyrazol-5(4*H*)-one (2c) L_3) is synthesized by condensing 3-methyl-1-phenyl-5-pyrazolone with substituted aromatic aldehydes as shown in Scheme 1 [27]. Three Ag(I) complexes have been prepared with the L_1, L_2, L_3 ligands as shown in Scheme 2. Based on physicochemical and spectral data (IR and ^{1}HNMR), structure of the synthesized compounds (**2a-c, Ag(I) complexes**) has been evaluated.

Infrared spectra

KBr disks registered mid-infrared spectra of L_1, L_2, L_3 and their metal complexes. As expected, with changes in band intensities and wave numbers, the absorption bands characteristic of L_1, L_2, L_3 acting as a monodentate unit are observed in the complexes. The proposed structures of the complexes must be considered prior to determining the assignments of the infrared spectra. Here, Ag(I) ion interacts with these monodentate ligands forming monomeric structure complexes in which the Ag(I) ion is four coordinated (Scheme 2) [27–30].

The complexes of three ligands with Ag(I) contain only one plane of symmetry and therefore the complexes that belong to C_S symmetry and show 159 vibrational fundamentals, and all vibrations are distributed between movements of the types $A^{\backslash}$ and $A_1^{\backslash\backslash}$, all of which are monodegenrate, infra—red and Raman active. The free ligand infrared spectrum shows bands at 1496, 1508 and 1550 cm^{-1} due to the stretching vibration of hydrazono (C=N) groups [31]. Comparing the Ag(I) IR spectrum with the free ligand spectrum, the transfer of (C=N) groups to lower frequency values (1512, 1515, 1523 and 1527 cm^{-1}) and the change in strength of (C=N) from

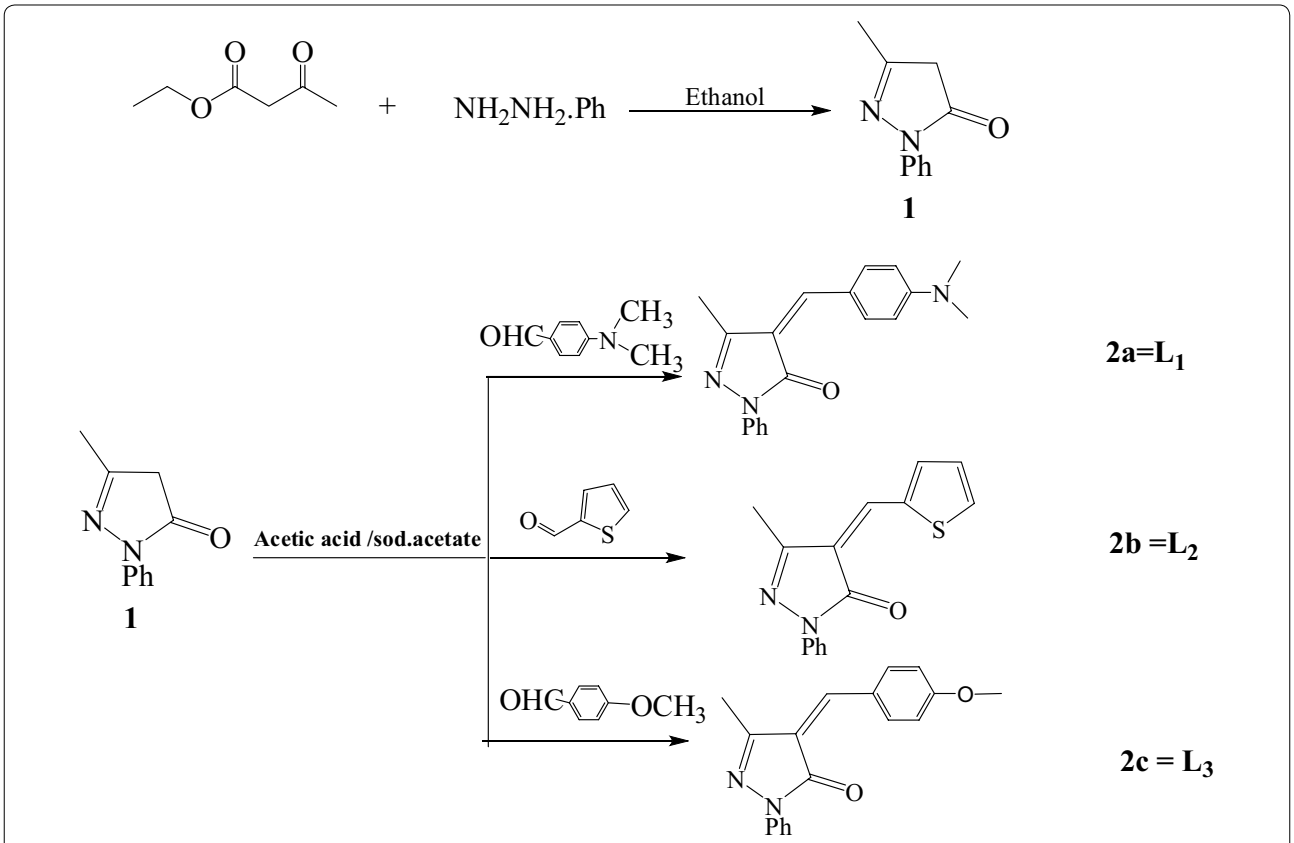

Scheme 1 Synthesis of 4-arylidene-3-methyl-1-phenyl-5-pyrazolone derivatives

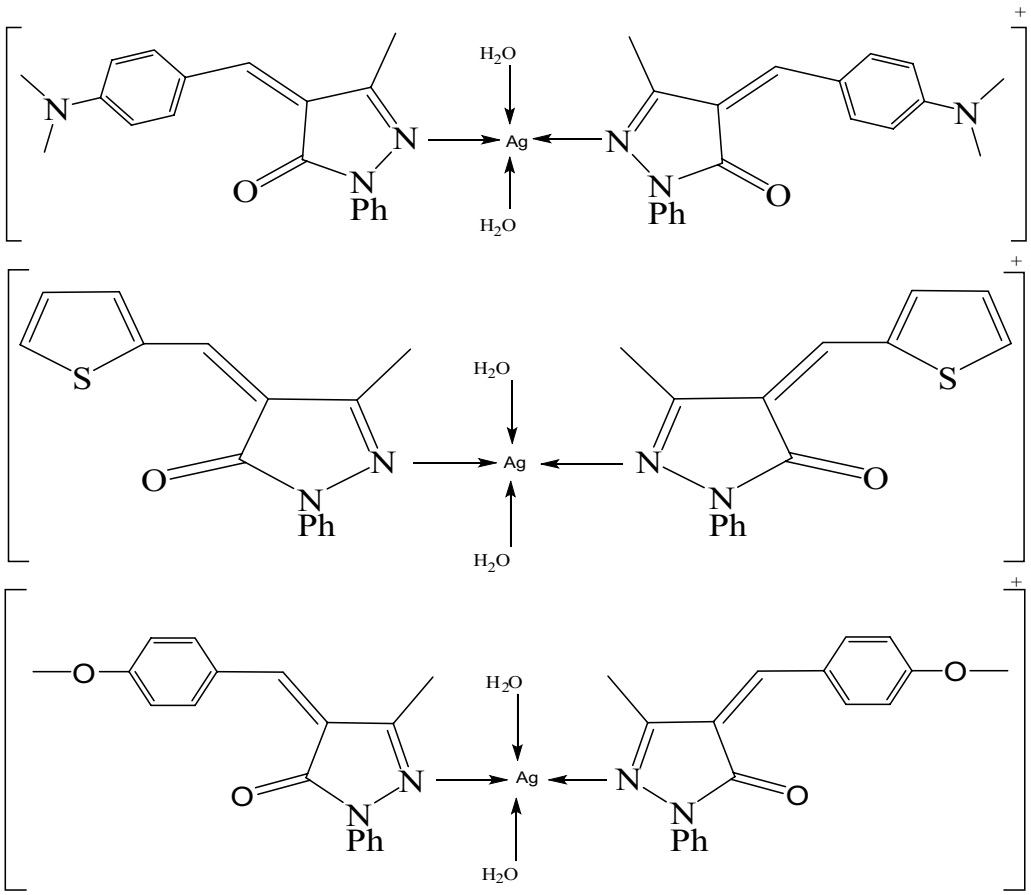

Scheme 2 The coordinationn mode of Ag (I) with three ligand

medium to strong (Fig. 1 and Table 1) which confirms that the ligand molecule coordinated with metal ions through the hydrazon nitrogen atom [31]. A medium wide band for the H_2O stretching vibrations of coordinated water molecules at 3379, 3364, and 3364 cm^{-1} [31];The stretching vibrations ν(C-H) of phenyl groups and $-CH_3$ units in these complexes are assigned as a number of bands in the region 3066–3100 cm^{-1} [11, 12]. The ν(C=O) vibration appears in the region of 1666–1685 cm^{-1}. The spectra of the isolated solid complexes revealed a number of new bands of different intensities for ν(M–N). The ν(Ag–N) bands observed at 813, 837 cm^{-1} for Ag(I)-L_1, at 748, 794 cm^{-1} for Ag(I)-L_2 and at 759, 779 cm^{-1} for Ag(I)-L_3 (Table 1) which are absent in the spectrum of free three ligands [30–32]. The coordinating water in the three complexes are characterized by the appearance of *ν*(Ag–O) at 577, 515, 544 cm^{-1}. Also the stretching vibrations at 813, 792, 779 cm^{-1} assigned to *ν*(Ag OH_2), sponsored coordinating water participation [32]. The suggested structural formulas are defined in Scheme 2 on the basis of the IR tests.

UV–Visible Spectra

The application of ultraviolet spectroscopy is more general and can be useful for all chelate structural determinations as they are all absorbed in this region [33]. Electronic absorption spectra confirmed the development of metal ligand complexes. Electronic absorption spectra L_1 for Ag(I), L_2 for Ag(I) and L_3 for Ag(I). Complexes within the spectrum of wavelengths between 200 and 800 nm are described in Additional file 1: Table S1 and Fig. 2. The free three-ligand UV spectrum (L_1, L_2 and L_3) displays bands at 281, 297 and 297 nm that are assigned respectively to π-π*. And displays bands allocated to n-π * transitions at 330 nm. The modification of the reflectance band to higher (bathochromic shift) and lower values (hypochromic shift) and the appearance of new bands for complexes has resulted in the release of three ligands' complex actions towards metal ions. Complexes also present bands within the range 410–480 nm which can be due to the transition of ligand–metal charges for three ligands [34, 36]. The molar absorptivity (ε) values of the prepared metal

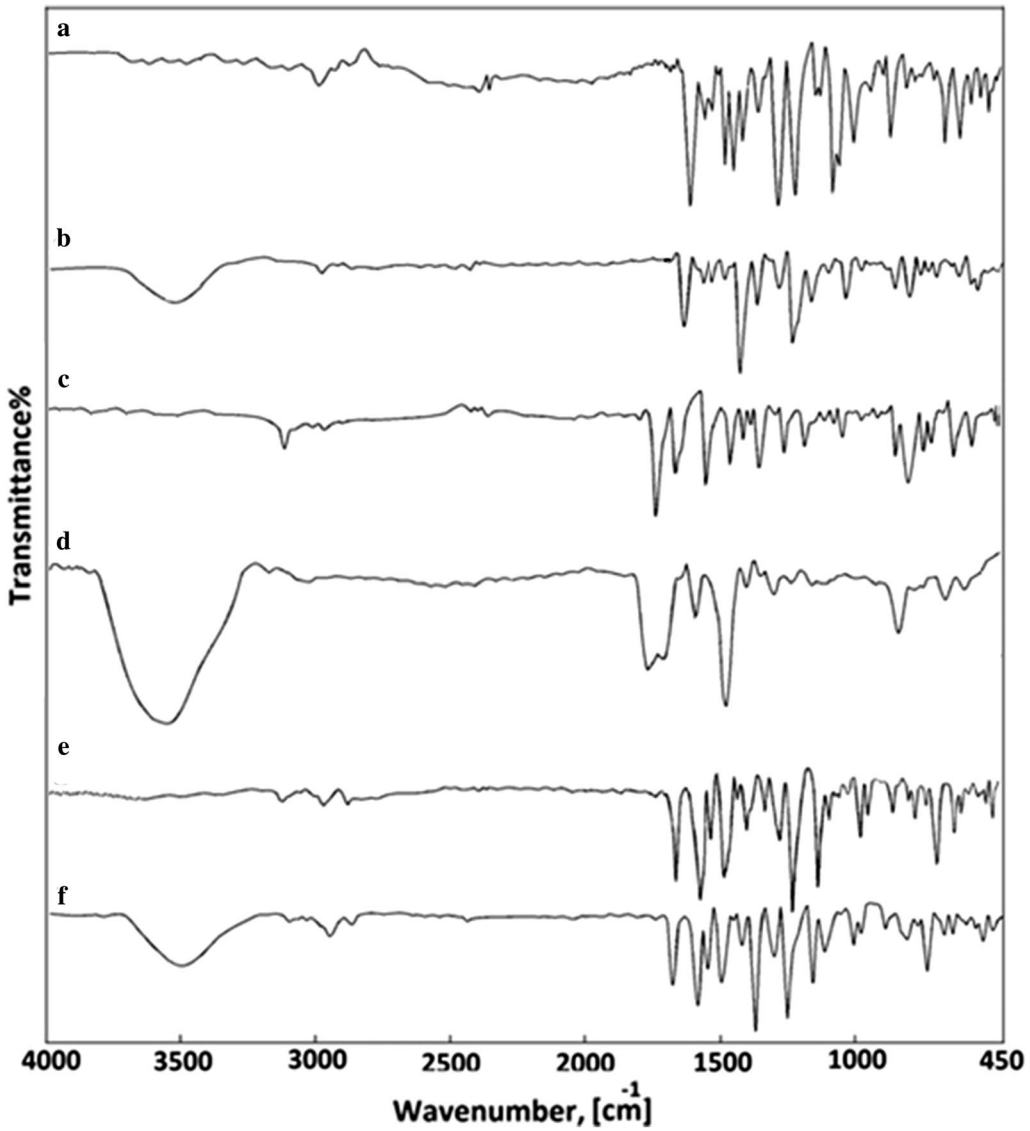

Fig. 1 Infrared spectra for **a** L_1, **b** $[Ag(L_1)_2(H_2O)_2]NO_3$, **c** L_2, **d** $[Ag(L_2)_2(H_2O)_2]NO_3.H_2O$, **e** L_3 and **f** $[Ag(L_3)_2(H_2O)_2]NO_3$

complexes under investigation were determined (Additional file 1: Table S1) using the relation: $A = \varepsilon cl$, where, A = absorbance, $c = 1.0 \times 10^{-3}$ M, l = length of cell (1 cm) [22]. The values of 10Dq (difference between t_{2g} and e_g) for the complexes were calculated by using the following Eq. $10Dq = E = hc\nu^{-}$ where E = energy, h = blank constant $= 6.626 \times 10^{-34}$ J.sec, $c = 3 \times 10^{10}$ cm/sec, ν^{-} = wave number cm^{-1} the data listed in Additional file 1: Table S1.

The ^{1}H NMR spectra

Suggested structure of the isolated Ag(I) complexes confirm about the efficiency of ^{1}H NMR spectra. Compared to the one of their complexes (Additional file 1: Table S2), the ^{1}H NMR spectra of new free three ligands in DMSO-d_6. The ^{1}H NMR spectra of L_1 and its metal complex shown in (Fig. 3a, b), the proton of (=CH-Ar) group observed in δ: 9.66 ppm and the protons of aromatic ring of (s, 9H, Aromatic–H) observed at δ: 7.14–7.97 ppm also the values of protons of -CH aliphatic observed in the range δ: 3.03–3.33 ppm (s, 6H, –N $(CH_3)_2$), the proton of (s, 3H, $-CH_3$) group observed in δ 2.28 ppm, no major differences were observed as opposed to the Ag(I) complex except that the signal is observed in 3.46 ppm due to H_2O molecules [36]. This supports the hypothesis that L_1 interacts as a monodentate ligand bound to the Ag(I) ion through the hydrazono nitrogen group. [37].

Table 1 Infrared frequencies (cm^{-1})[a] and tentative assignments[b] for (A) L_1, (B) $[Ag(L_1)_2(H_2O)_2]NO_3$, (C), L_2 (D) $[Ag(L_2)_2(H_2O)_2]NO_3.H_2O$, (E) L_3 and (F) $[Ag(L_3)_2(H_2O)_2]NO_3$

A	B	C	D	E	F	Assignments
-	$3379_{m,br}$	–	$3364_{m,br}$	–	$3364_{m,br}$	ν(O–H); coordinate H_2O
3100_w	3100_w	3066_w	3100_w	3099	3100	ν(C-H); aromatic
2900	2900	2890	2885	2901	2900	ν(C-H); aliphatic
1670_{ms}	1666_m	1681_s	$1685_{s,sh}$	1678_m	1678_m	ν(C = O)
1550_s 1400_m	1523_m 1410_s	1496_m 1408_m	1527_m 1381	1508_s 1427_{vw}	1520_s 1415	ν(C = N) ν(C = C)
1319_s –	1319_s 1188_s	1300_s -	1311_w 1165_m	1311_{sh} -	1311_m 1172_s	δ_b(-CH_2), ν(NO_3^{-1})
1122_s 1018_w	1122_s 1018_w	1130_m –	1104_{vw} –	1110_w –	1130_m –	ν(C–C), ν(C-N)
–	–	1056_w	1099_{sh}	–	–	ν(C = S)
954_w 943_{vw}	995_w 995_m	991_s 921_w	941_{vw} 910_{vw}	988_w 938_s	985_w 965_{sh}	–CH-bend; phenyl
–	813_m	–	792 m	–	779_m	ν(Ag ←OH_2)
–	577w	–	515w	–	544w	ν(Ag–O)
–	524w	–	498w	–	488w	ν(Ag–N)

[a] s = strong, w = weak, sh = shoulder, v = very, br = broad, [b]ν = stretching and δ = bending

The ^{1}H NMR spectra of L_2 and its Ag(I) complex shown in (Fig. 3c, d), the proton of (=CH-Ar) group observed in δ: 8.25 ppm and, the protons of aromatic ring of (s, 8H, Aromatic–H) observed at δ: 7.39–7.91 ppm [38]. The proton of (s, 3H, $–CH_3$) group observed in δ 2.30 ppm, simple differences are shown in comparison to the metal complex and the signal is observed in π: 3.47 ppm due to H_2O molecules. This reinforces the hypothesis that L_2 reacts via the hydrazono nitrogen group as a monodentate ligand bound to the Ag(I) ion. The ^{1}H NMR spectra of L_3 and its Ag(I) complex shown in (Fig. 3 (E, F)), the proton of (=CH-Ar) group observed in δ: 8.71 ppm and the protons of aromatic ring of (s, 9H, Aromatic–H) observed at δ: 7.18–7.46 ppm also the values of protons of -CH aliphatic observed in the range δ: 3.31 ppm (s, 3H, $–O-CH_3$), the proton of (s, 3H, $–CH_3$) group observed in δ 2.33 ppm, no major variations were noticed as opposed to the Ag(I) series. This supports the assumption that L_3 reacts as a monodentate ligand bound to the Ag(I) ion via the hydrazone nitrogen group.

Thermal studies

The thermal degradation of ligand (L_1) began at 190 °C and decay occurs at various temperatures at 310, 544 °C at one stage (Additional file 1: Fig. S1a). This step is accompanied by a net weight loss of 92.36 percent, equivalent to the predicted 92.07 percent. Corresponding to the loss of $8C_2H_2 + NH_3 + CO + N_2$ molecule and 95.65KJ mol^{-1} (endothermic) activation energy. The residue value decomposes at a height of 800 °C and the actual losing weight at this point is 7.64 percent, close to the estimated 7.86 percent equal to 2C. The $[Ag(L_1)_2(H_2O)_2]NO_3$ complex decomposed in two steps (Additional file 1: Fig. S1b), The first one begins at a limit of 189 °C and is followed by a 33.378 percent weight loss leading to a $9C_2H_2 + 2H_2O$ loss similar to the estimated value of 33.062 percent with an activation energy of 34.37 kJ mol^{-1}. The second step occurs at 366 and 562 °C followed by a weight loss of 52.79 percent; equivalent to a value of $8C_2H_2 + 4HCN + NO + 2N_2O$, potentially similar to the measured value of 53.798 percent. The residue value proceeds at 931 °C and the overall weight loss from this stage is 13.474 percent, referring to Ag, similar to the 13.14 percent estimated value (Table 2).

The ligand (L_2) degradates at 273, 475 °C. This stage is followed by a complete loss of weight of 86.70 percent, close to 86.56 percent of the estimated value (Additional file 1: Fig. S1c). Equivalent to $6C_2H_2 + SO + N_2$ loss and 31.93 kJ mol^{-1} (endothermic) activation energy. Decomposition of the residual value occurs at 771 °C and the real weight loss from this stage is 13.30 percent, similar to the estimated value of 13.43 percent corresponding to 3C. The $[Ag(L_2)_2(H_2O)_2]NO_3.H_2O$ complex decomposes at two levels of decay (Additional file 1: Fig. S1d), the first phase occurs at 99 °C and is followed by a weight loss of 2.08 per cent relating to the removal of H_2O, activation energy of 79.28 kJ mol^{-1}. The second step of decomposition occurs at temperature is 203, 528 and is accompanied by a weight loss of 75.90%; corresponding to the value of $10C_2H_2 + 4HCN + 2H_2O + NO_2 + SO + SO_2$ theoretically, close to the calculated value 76.404%.

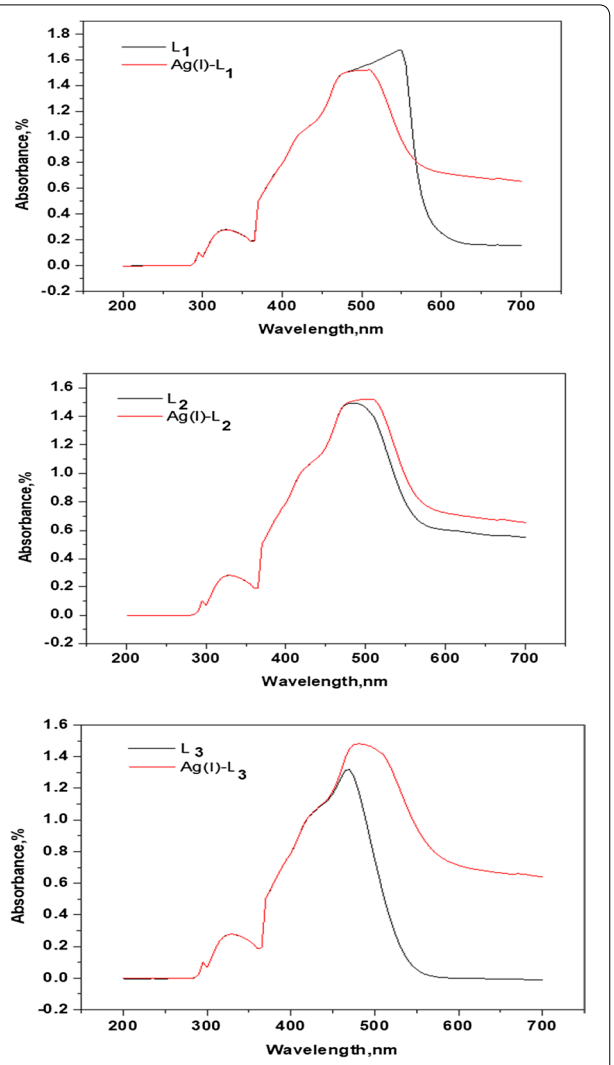

Fig. 2 Electronic absorption spectra for L_1, $[Ag(L_1)_2(H_2O)_2]NO_3$, L_2, $[Ag(L_2)_2(H_2O)_2]NO_3.H_2O$, L_3 and $[Ag(L_3)_2(H_2O)_2]NO_3$

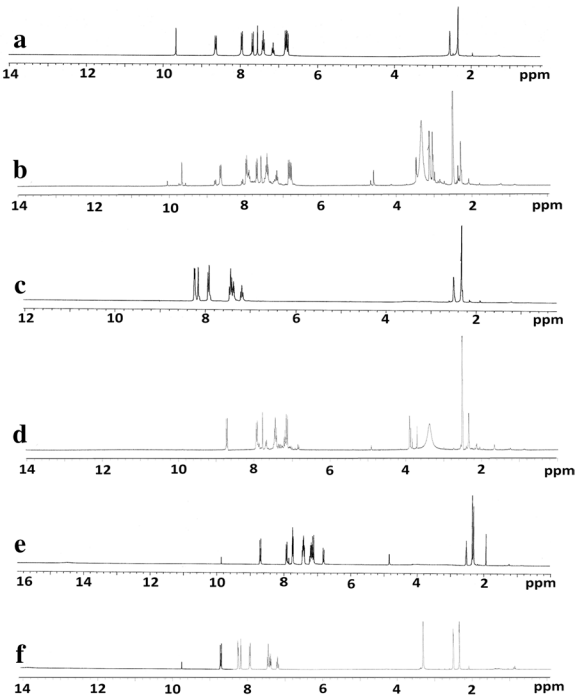

Fig. 3: ^{1}H NMR spectra for **a** L_1, **b** $[Ag(L_1)_2(H_2O)_2]NO_3$, **c** L_2, **d** $[Ag(L_2)_2(H_2O)_2]NO_3.H_2O$, **e** L_3 and **f** $[Ag(L_3)_2(H_2O)_2]NO_3$

The Residue value decomposition occurs at maximum 881 °C and the actual weight loss from this step is 23.35%, corresponding to Ag + 6C, close to the calculated value 23.596%.

The thermal decay of L_3 happens in two phases of degradation (Additional file 1: Fig. S1e), the first step arises at 291 °C and is followed by a weight loss of 70.55 percent leading to a loss of $8C_2H_2$ similar to the measured value of 71.23 per cent with activation energy of 35.31 kJ mol^{-1}. The second step occurs at 518 °C and is accompanied by a weight loss of 28.604%; corresponding to the value of $2CO + N_2$ theoretically, close to the calculated value 28.67%. The $[Ag(L_3)_2(H_2O)_2]NO_3$ degradation takes place in two stages (Additional file 1: Fig. S1f), the first occurs at 244 °C and is accompained by a weight loss of 51.071% corresponding to loss of $14C_2H_2 + 2H_2O$ close to the calculated value 50.60% with an activation energy 15.31 kJ mol^{-1}. The second one begins at 543 °C and is followed by a weight loss of 30.17%; corresponding to $C_2H_2 + CO + 2HCN + 3NO_2$ theoretically, close to the calculated value 31.25%. The Residue remains at 677 °C and the actual weight loss is 17.76%, equal to Ag + 3C, close to the calculated value 18.15%.

Kinetic data

The kinetic parameters (activation energy, E*, entropy, ΔS*, enthalpy, ΔH*, and Gibbs free energy, ΔG*) have been evaluated by using the two mentioned methods in the literature [39, 40] and shown in Additional file 1: Fig. S2 and listed in Table 3. The correlation coefficient for Arrhenius plots of thermal degradation stages were found to be in the range 0.943–0.985, revealing a good fit with linear function. The activation energies of decomposition were observed to be in the range 7.44–154.69 kJ mol^{-1}. The negative values of ΔS* indicate that the activation complex has a more ordered structure than the reactants or the reactions are slow. The positive ΔH* values postulate an endothermic nature of the formed complexes. The greater positive values of E* indicate that the processes involving in translational, rotational, vibrational states and a changes in mechanical potential

Table 2 Thermogravimetric data of L_1, L_2,L_3 and their metal complexes

Compounds	Decomposition	DTG $_{max}$ (°C)	% Estimated (calculated)		Assignment
			Mass loss	Total mass loss	Lost species
L_1	First step	190,310,544,800	92.36 (92.07)	92.36 (92.07)	$8C_2H_2+CO+NH_3+N_2$
305.19, $C_{19}H_{19}ON_3$	Residue		7.64 (7.86)		2C
$[Ag(L_1)_2(H_2O)_2]NO_3$	1st step	189	33.378 (33.062)	86.526 (86. 86)	$9C_2H_2+2H_2O$
816.65, $AgC_{38}H_{42}N_7O_7$	Second step	366,562,	52.79 (53.798)		$8C_2H_2+4HCN+NO+2NO_2$
	Residue	807,931	13.474 (13.14)		Ag
L_2	First step	273,475,771	86.70(86.56)	86.7(86.56)	$6C_2H_2++SO+N_2$
268, $C_{15}H_{12}N_2OS$	Residue		13.30(13.43)		3C
$[Ag(L_2)_2(H_2O)_2]NO_3.H_2O$	First step	99	2.08 (2.37)	75. 90 (76.404)	H_2O
760.59, $AgC_{30}H_{30}N_5O_8S_2$	Second step	203,528	73.82 (74.034)		$10C_2H_2+4HCN+2H_2O+NO_2+SO+SO_2$
	Residue	881	23.35 (23.596)		$Ag+6C$
L_3	First step	120, 291	70.55(71.23)	99.834 (99.99)	$8C_2H_2$
292, $C_{18}H_{16}O_2N_2$	Second step	518	28.604 (28.76)		$2CO+N_2$
$[Ag(L_3)_2(H_2O)_2]NO_3$	First step	244	51.071 (50.60)	82.241 (81.85)	$14C_2H_2+2H_2O$
790.57, $AgC_{36}H_{36}N_5O_9$	Second step	534	31.17 (31.25)		$C_2H_2+CO+2HCN+3NO_2$
	Residue	677	17.76 (18.15)		$Ag+3C$

energy for complexes and reflect the thermal stability of the complexes [41].

Mass spectra

The principle of a mass spectrometer focuses on the separation of fragments of ions based on the distribution of these ions with the mass to charge ratio (m/z). The L_1, L_2, L_3 fragmentation patterns and their complexes were obtained from the mass spectra, and were in good agreement with the structure suggested. The L_1 showed molecular ion peak ($M^{+\cdot}$) with m/z = 305 (100%). The molecular ion peak [a] losses C_2H_6N to give fragment [b] at m/z = 261 (3.13%), then [b] losses C_6H_4 to give fragment [c] at m/z = 185 (2.98%) and [c] losses CH_3O to give [d] at m/z = 154(0.66%). The molecular ion peak [a] losses $C_9H_{11}N$ to give fragment [e] at m/z = 172 (29.92%) and this [e] losses C_7H_8O to give fragment [f] at m/z = 64 (2.08%) (Fig. 4), (Scheme 3). Fragmentation pattern of the complex $[Ag(L_1)_2(H_2O)_2]NO_3$ is given as an example in (Fig. 4), Additional file 1: Scheme S1. The molecular ion peak [a] appeared at m/z = 816 (20.5%) losses $C_{18}H_{22}N_2$ to give [b] at m/z = 514 (17.7%) and it losses $C_2H_6O_2$ to give [c] at m/z = 452 (11.7%). The L_2 molecular ion peak [a] appeared at m/z = 268 (100%) losses C_4H_3S to give [b] at m/z = 185 (14.60%) then it losses CH_3O to give [c] at m/z = 154 (0.2%), molecular ion peak[c] lossC_6H_5 to give [d] at m/z = 77(28.34%) and molecular ion peak [d] losses CH to give [e] at m/z = 64 (4.89%).(Fig. 4), Scheme 4. Fragmentation pattern of the complex $[Ag(L_2)_2(H_2O)_2]NO_3.H_2O$ is given as an example in (Fig. 4), Additional file 1: Scheme S2. The molecular ion peak [a] appeared at m/z = 760 (35%) losses $C_{10}H_8S_2$to give [b] at m/z = 532 (5%) and it losses $C_2H_6O_2$ to give [c] at m/z = 470 (12%). The L_3 molecular ion peak [a] appeared at m/z = 292 (100%) losses CH_3O to give [b] at m/z = 261 (4%) then [a] losses C_6H_4 to give [c] at m/z = 185 (21.73%), molecular ion peak[c] loss CH to give [d] at m/z = 172(6.8%) and molecular ion peak [d] losses CH_3O to give [e] at m/z = 141 (1.2%).(Fig. 4), Scheme 5. Fragmentation pattern of the complex $[Ag(L_3)_2(H_2O)_2]NO_3$ is given as an example in (Fig. 4), Additional file 1: Scheme S3. The molecular ion peak [a] appeared at m/z = 790 (65%) losses $C_2H_6O_2$to give [b] at m/z = 692 (2%), it losses $C_{12}H_8$ to give [c] at m/z = 540 (12.5%) and molecular ion peak [c] losses C_2H_2 to give [d] at m/z = 514 (25.3%) [42].

Biological activity studies

Antimicrobial studies

The antimicrobial efficacy of L_1, L_2, L_3 and their free ligand complexes are explored in this experiment. Studies were conducted on *E. Coli* ATCC11229, *Coliform* ATCC8729, *S. aureus* ATCC6538, and *Salmonella typhi* ATCC14028 and fungal species as *A. niger* and *P. expansum* screening was tested against and examination and evaluation of the prepared complexes [42]. The same results were reported for *E. Coli* ATCC11229 of Ag(I)-L_2 and Ag (I)-L_1 followed by Ag(I)-L_3 considers that the lowest findings are equivalent to those of other complexes. The effect of free ligands on this strain has been shown to be below its complex and can be organized according to the sensitivity of the strains L_2, L_3 and L_1 in the following ascending order. The effect of Ligands and their

Table 3 Thermal behavior and kinetic parameters determined using the Coats–Redfern (CR) and Horowitz–Metzger (HM) operated for L_1, L_2, L_3 and their complexes

Compounds	Decompositi range(K)	T_s(K)	Method	Parameter					R^a	SD^b
				E^* (kJ mol^{-1})	A (s^{-1})	ΔS^* (J mol^{-1} K^{-1})	ΔH^* (kJ mol^{-1})	ΔG^* (kJ mol$^{-1)}$		
L_1	673–905	817	CR	95.656	69.368×10^3	− 432.844	88.863	442.497	0.970	0.187
			HM	116.813	30.233×10^3	− 425.910	110.020	457.988	0.984	0.065
$[Ag(L_1)_2(H_2O)_2]NO_3$	373–573	462	CR	34.379	3.390×10^2	− 393.344	30.537	212.262	0.984	0.116
			HM	38.825	2.621×10^3	− 410.348	34.983	224.564	0.970	0.087
L_2	453–645	546	CR	31.931	37.451	− 373.640	27.391	231.398	0.943	0.207
			HM	40.983	672.979	− 397.656	36.443	253.563	0.945	0.112
$[Ag(L_2)_2(H_2O)_2]NO_3.H_2O$	689–881	801	CR	79.284	6.618×10^3	− 413.475	72.624	403.817	0.945	0.220
			HM	93.856	113.45×10^3	− 437.099	87.196	437.312	0.940	0.116
L_3	438–630	564	CR	35.317	1.185×10^2	− 382.948	30.627	246.610	0.960	0.182
			HM	48.603	2.847×10^3	− 409.379	43.913	274.803	0.952	0.106
$[Ag(L_3)_2(H_2O)_2]NO_3$	365–685	497	CR	15.316	0.758	− 342.002	11.183	181.158	0.981	0.089
			HM	22.370	0.119×10^2	− 364.917	18.237	199.601	0.985	0.054

[a] Correlation coefficients of the Arrhenius plots and [b]Standard deviation

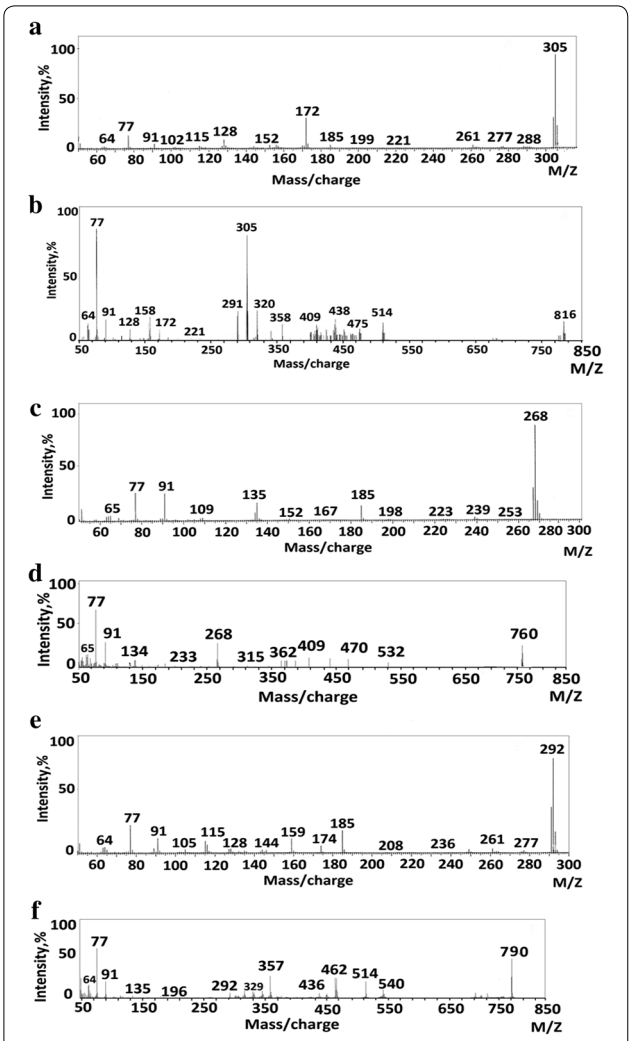

Fig. 4 Mass spectra diagrams for (A) L_1, (B) $[Ag(L_1)_2(H_2O)_2]NO_3$, (C), L_2 (D) $[Ag(L_2)_2(H_2O)_2]NO_3.H_2O$, (E) L_3 and (F) $[Ag(L_3)_2(H_2O)_2]NO_3$

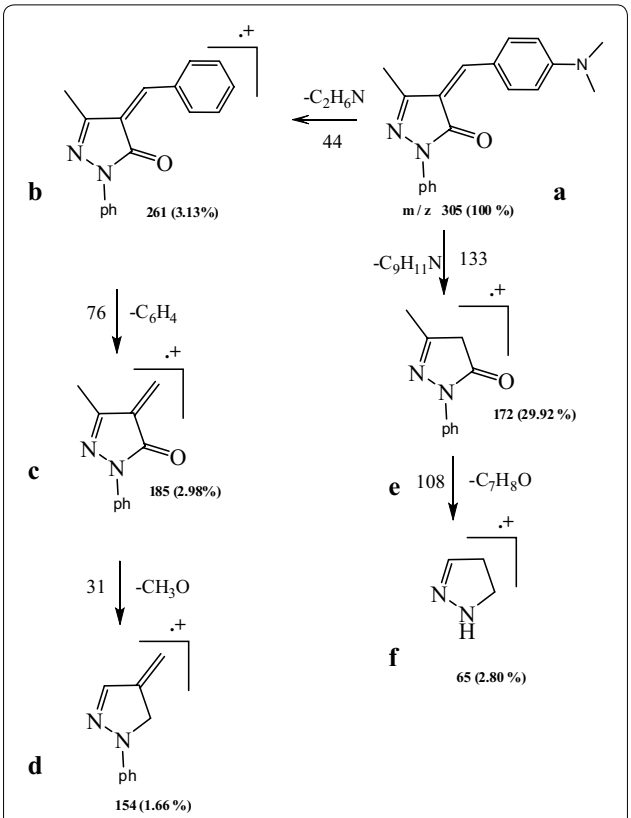

Scheme 3 Fragmentation pattern of L_1

complexes on *Coliform* ATCC8729 showed that Ag(I)-L_2 is highly important, giving 25.12 mm respectively. Although the remaining complexes showed lower results than the L_2 complexes. The results obtained in Table 4 and Fig. 5 showed that lower activity on the same strain and these results ensured that free ligand complexes were more active than free ligand complexes. In gram + ve bacteria, *S. aureus* ATCC6538, Highly important antibacterial activity of metal complexes with L_1 followed L_3 complex. The lesser activity from ligand L_2 and its complex. The antibacterial activity of metal complexes on *Salmonella typhi* ATCC14028 showed a good activity against (gram −ve), that recorded the best results Ag(I)-L_3 > Ag(I)-L_1 > Ag(I)-L_2 respectively. The action of the free ligands on gram −ve bacteria has yielded results lower than their complexes which give respectively 12.6, 11.43 and 7.8 mm, L_3, L_1, L_2. The presence of different ligands and other complexes on both fungal strains of the testes, *A. niger* recorded that Ag(I)-L_3 showed a significant difference the highly results (20 ± 2.6) though free L_3 results showed less than its complex. Others did not show any activity against tested fungi (*A. niger*). The effect of various significant ligands and other complexes on *P. expansum* did not show any activity whereas the the highest broad spectrum of activity on the same test strain showed the best results on L_1 and its complexes [42].

Normal antibiotic efficacy of antimicrobials (AMC, CTX, NS, FU). The AMC mixture give the effective against *E. coli*, *Coliform*, *S. aureus* and NS high inhibitory activity on *A. niger*. Other antibiotics have shown no action on other microorganisms. Eventually, the bacterial strains showed a varied response to the three free ligands and their complex antimicrobial activity, but the results indicated that the high activity of ligand complexes was better than their free ligands. The two fungal strains are more resistant to synthesis ligands and their complexes than bacterial strains [42–46].

Determination of MIC for the most sensitive organisms

The artificial ligands and their complexes developed the biological efficacy towaeds the more resistant

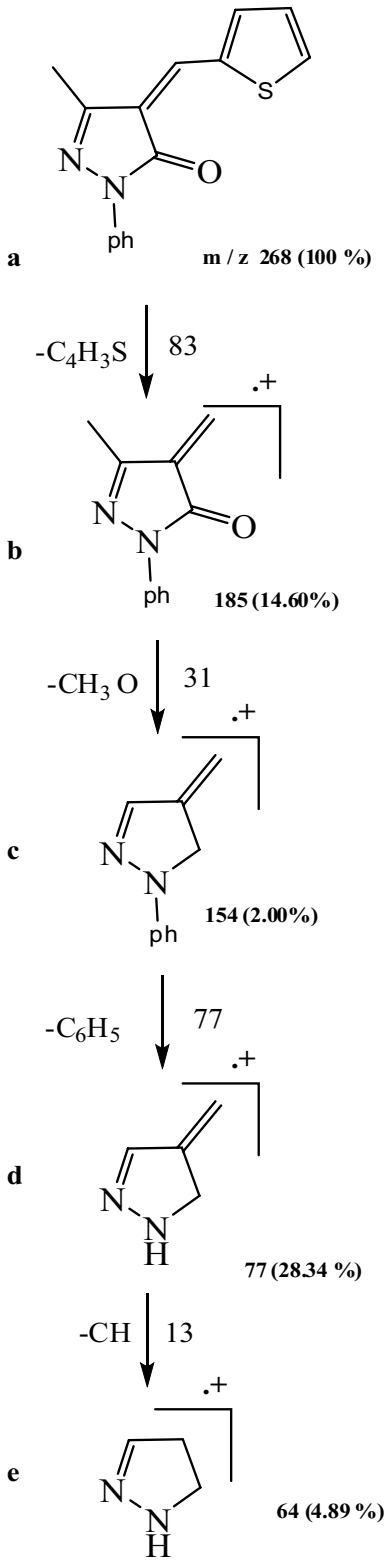

Scheme 4 Fragmentation pattern of L_2

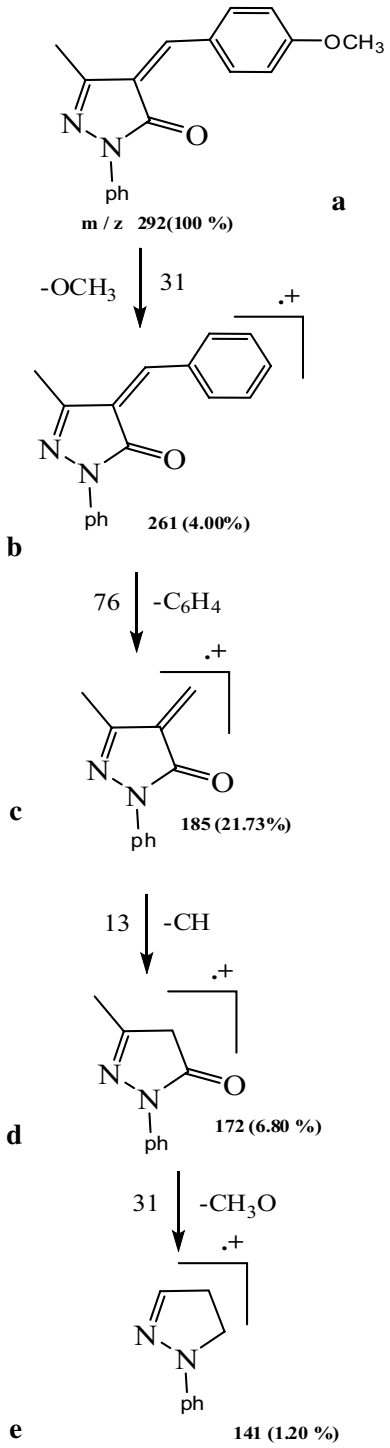

Scheme 5 Fragmentation pattern of L_3

bacteria and fungi (Table 5A–D) and Fig. 6). The order of The lowest MIC for in case of *E. coli* decrease in order: L_1 = Ag (I) – L_3 (0.02 mg/100 mL)$^{>}$ L_3

Table 4 The inhibitation diameters zone values (mm) for L_1, L_2, L_3 and its complexes

Compounds		Microbial species					
		Bacteria				Fungi	
		E. coli	*Coliform*	*S. aureus*	*Salmonella typhi*	*A.niger*	*P.expansum*
L_1		$10^{+1} \pm 1.1$	$11^{+1} \pm 1.8$	$12.5^{+1} \pm 0.89$	$11.43^{+3} \pm 0.79$	NA	$20^{+3} \pm 1.3$
L_1 / Ag(I)		$29.33^{+2} \pm 1.58$	$18.65^{+2} \pm 1.45$	$22.6^{+1} \pm 1.88$	$21.6^{+3} \pm 1.98$	NA	$16^{+3} \pm 0.75$
L_2		$14.66^{+1} \pm 1.1$	$15.13^{+1} \pm 1.9$	$6.25^{+1} \pm 0.81$	$7.8^{+1} \pm 0.54$	NA	NA
L_2 / Ag(I)		$29.6^{+2} \pm 1.75$	$25.12^{+3} \pm 1.33$	$9.5^{+1} \pm 0.74$	$20^{+3} \pm 2.1$	NA	NA
L_3		$11.2^{+1} \pm 1.4$	$10.5^{+1} \pm 0.95$	$13.6^{+1} \pm 1.3$	$12.6^{+3} \pm 0.78$	$14^{+2} \pm 0.75$	NA
L_3 / Ag(I)		$22.16^{+1} \pm 2.4$	$15.32^{+1} \pm 1.3$	$20.8^{+1} \pm 2.2$	$22^{+3} \pm 2.2$	$20^{+3} \pm 2.6$	NA
$AgNO_3$			–	–	–	–	–
Control (DMF)		–	–	–	–	–	–
Standard	Nystain	–	–	–	–	11 ± 1.1	00
	Fluconazole	–	–	–	–	00	00
	Amoxycillin/Clavulanic	17 ± 1.1	14 ± 1.3	19 ± 1.8	00	–	–
	Cetaxime	00	00	00	00	–	–

Statistical significance P^{NS} – P not significant, $P > 0.05$; P^{+1} – P significant, $P < 0.05$; P^{+2} – P highly significant, $P < 0.01$; P^{+3} – P very highly significant, $P > 0.001$; Student's *t*-test (Paired)

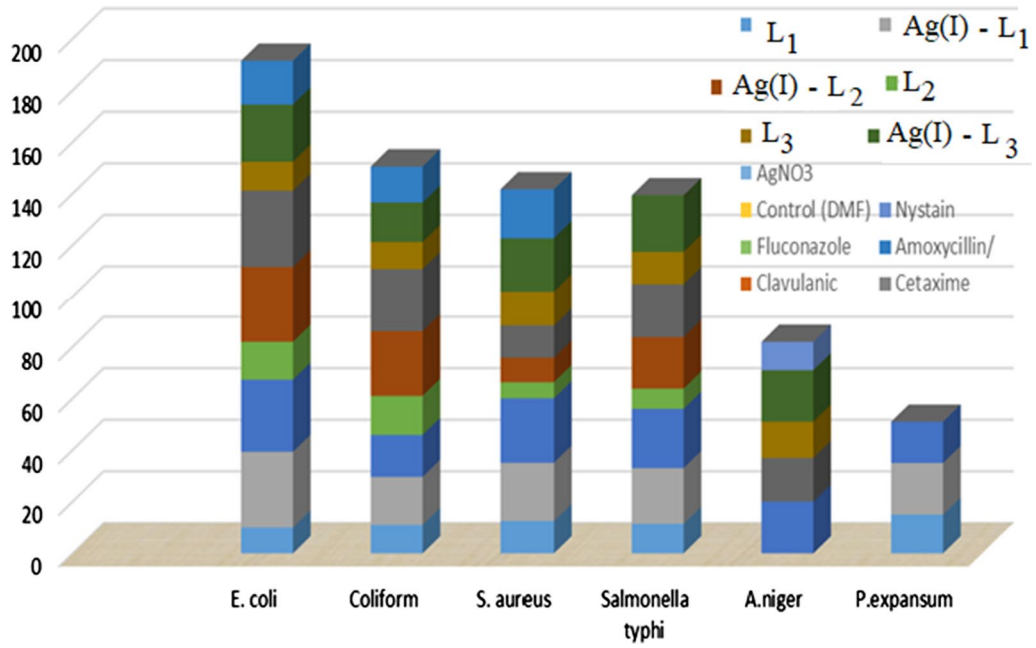

Fig. 5 Statistical representation for biological activity of L_1, L_2, L_3 and its metal complexes

(0.05 mg/100 mL)˃ Ag (I) – $L_1 = L_2$ (0.07 mg/100 mL) ˃ Ag (I) – L_2 (0.1 mg / 100 mL) [42], *Coliform* decrease in order: Ag (I) – L_2 (0.02 mg/100 mL) ˃ Ag (I) – $L_3 = L_2$ (0.07 mg/100 mL) ˃ $L_1 =$ Ag (I) – $L_1 = L_3$ (0.1 mg/100 mL). *Salmonella typhi* showed that, the amazing results of ligands and its complexes: L_2, Ag(I) – L_2 = Ag(I) – L_1 (0.02 mg/100 mL) ˃ Ag (I) – $L_3 = L_1$ (0.05 mg/ 100 mL) ˃ L_3 (0.1 mg/ 100 mL), *S. aureus* order: L_3 = Ag(I) – L_2 = Ag(I) – $L_1 = L_1$ = Ag(I) –L_3 (0.1 mg/ 100 mL) ˃ L_2 (0.05 mg/ 100 mL). Table 5E, F and Fig. 6 data showed that the lowest MIC for the two strains measured at conc. 0.02 mg/100 mL. Although MIC at complex L_3 was recorded by *A.niger*, the same result was recorded on Ag(I)—L_3 at conc. 0.02 mg/100 mL. Ligand L_1 and its complexes demonstrate the strongest MIC on *P. expansum*, although no behavior is displayed

Table 5 (A) Of One-way ANOVA: *E. coli* vs MIC Compounds. (B) Of One-way ANOVA: Coliform versus MIC Compounds. (C) Of One-way ANOVA: *S. aureus* vs MIC Compounds. (D) Of One-way ANOVA: *Salm. typhi* vs MIC Compounds. (E) Of One-way ANOVA: *A. niger* vs MIC Compounds. (E) Of One-way ANOVA: *A. niger* vs MIC Compounds. (F) Of One-way ANOVA: *P.expansum* vs MIC Compounds

(A)

Grouping information using the fisher LSD method

Compounds	N	Mean	Grouping
L_1	3	0.02	A
L_3/Ag(I)	3	0.02	A
L_3	3	0.05	B
L_1/Ag(I)	3	0.07	B
L_2	3	0.07	B
L_2/Ag(I)	3	0.10	C

(B)

Grouping information using the fisher LSD method

Compounds	N	Mean	Grouping
L_2/Ag(I)	3	0.02	A
L_2	3	0.07	C
L_3/Ag(I)	3	0.07	C
L_1	3	0.10	D
L_1/Ag(I)	3	0.10	D
L_3	3	0.10	D

(C)

Grouping information using the fisher LSD method

Compounds	N	Mean	Grouping
L_3/Ag(I)	3	0.05	A
L_3	3	0.05	A
L_2/Ag(I)	3	0.07	B
L_1/Ag(I)	3	0.10	C
L_1	3	0.10	C
L_2	3	0.10	C

(D)

Grouping information using the fisher LSD method

Compounds	N	Mean	Grouping
L_1/Ag(I)	3	0.02	A
L_2	3	0.02	A
L_2/Ag(I)	3	0.02	A
L_1	3	0.05	B
L_3/Ag(I)	3	0.05	B
L_3	3	0.10	C

(E)

Grouping information using the fisher LSD method

Compounds	N	Mean	Grouping
L_3/Ag(I)	3	0.02	A
L_3	3	0.02	A
L_2/Ag(I)	3	0.0	B

Table 5 (continued)

(E)			
Grouping information using the fisher LSD method			
Compounds	**N**	**Mean**	**Grouping**
L_2	3	0.0	B
L_1/Ag(I)	3	0.0	B
L_1	3	0.0	B
(F)			
Grouping information using the fisher LSD method			
Compounds	**N**	**Mean**	**Grouping**
L_1/Ag(I)	3	0.02	A
L_1	3	0.02	A
L_3/Ag(I)	3	0.0	B
L_3	3	0.0	B
L_2/Ag(I)	3	0.0	B
L_2	3	0.0	B

Means that do not share a letter are significantly different

Fisher 95% Simultaneous Confidence Intervals

by the other compounds and their complexes. These findings ensured that the activity of synthetic ligands and their complexes on pathogenic bacteria and fungi demonstrated a minimum inhibitor concentration (MIC) for the most vulnerable pathogens. [42, 47, 48].

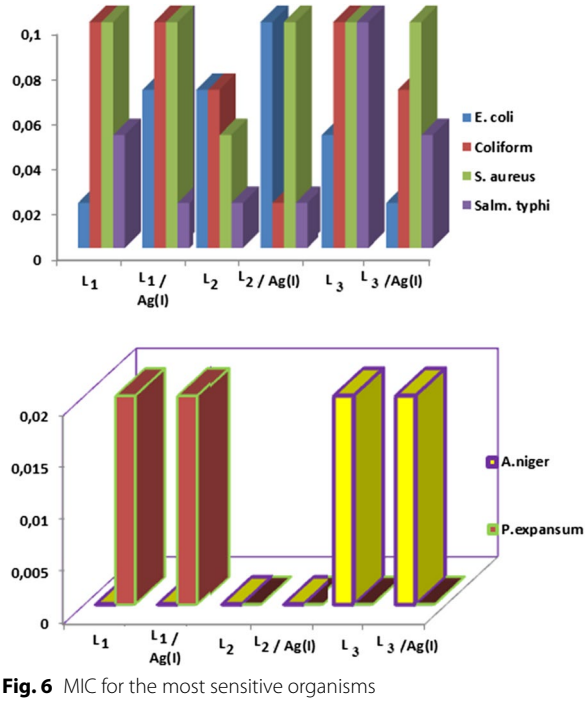

Fig. 6 MIC for the most sensitive organisms

Conclusion

Development and characterisation of three novel complexes of some replaced pyrazole derivatives as ligands (4-(4-dimethylamino benzylidene)-3-methyl-1-phenyl-1*H*-pyrazol-5(4*H*)-one (2a) L_1, 4-(4-Thiophene)-3-methyl-1-phenyl-1*H*pyrazol-5(4*H*)-one (2b) L_2, 4-(4-methoxy benzylidene)-3-methyl-1-phenyl-1*H*pyrazol-5(4*H*)-one (2c) L_3) with Ag(I) was achieved using physicochemical and spectroscopic methods.. In the resulting complexes, L_1, L_2, and L_3 were bound by the nitrogen atom to the metal ion via ν(C = N). For the three ligands and their complexes, thermogravimetric kinetic parameters and their differential were evaluated using the Coats-Redfern and Horowitz-Metzger equations. Metal complexes exhibited higher inhibition against all tested microorganisms and pathogenic bacteria and fungi and were the most susceptible pathogens with a minimum inhibitory concentration (MIC).

Methods

Chemistry

Analytical grade reagents, commercially available from multiple suppliers and used without further purification, were all the chemicals used in the complex preparation. Synthesized compounds and their complexes have been characterized by elemental analysis, magnetic and spectroscopic methods (IR, ^{13}C, $^{1}HNMR$, mass) and thermal analysis using the known apparatuses [42].

Synthesis of the ligands

Common 3-methyl-1-phenyl-5-pyrazolone synthesis technique (1)

Pure ethyl acetoacetate (0.05 mol, 6.2 mL) was mixed with pure phenyl hydrazine (0.05 mol, 5 mL), 0.5 mL of acetic acid was added, according to knowm method [42]. Methyl phenyl pyrazolone was obtained as colorless crystals, 127 °C melting point and 83.6 percent yield [27].

Specific method for preparing derivatives of 4-arylidene-3-methyl-1-phenyl-5-pyrazolone (2a-c)

The oil bath heated a mixture of 1-aryl-3-methyl-5-pyrazolone (0.01 mol, 1.74 g) and replaced aromatic aldehydes (0.012 mol) at 150–160 °C for 2-4hrs. TLC has tracked the progress of the reaction using ethyl acetate: hexane (9:1) as solvent. The mixture was cooled, triturated and washed off with ether (20 mL). The colored residue was recrystallized from ethanol to provide the corresponding 4-arylidene-3-methyl-1-phenyl-5-pyrazolone (2a-c) as colored products, respectively [28].

4-(4-dimethylamino benzylidene)-3-methyl-1-phenyl-1*H*-pyrazol-5(4*H*)-one (2a) L_1.

4-(4-Thiophene)-3-methyl-1-phenyl-1*H*pyrazol-5(4*H*)-one (2b) L_2.

4-(4-methoxy benzylidene)-3-methyl-1-phenyl-1*H*pyrazol-5(4*H*)-one (2c) L_3.

4-(4-dimethylamino benzylidene)-3-methyl-1-phenyl-1*H*-pyrazol-5(4*H*)-one (2a) L_1

Brick Red, mp = 170 °C, yield 83% IR (KBr, *ν*, cm^{-1}): 3444 (OH), 1670 (C = O), and 1550 $cm^{-1.}$ ^{1}H NMR (DMSO-d_6, 300 MHz): δ = 2.28 (s, 3H, CH_3), 3.03 (s, 6H, -N $(CH_3)_2$), 7.14 (S, 1H, = CH-Ar), 9.66 (d, 3H, Ar–H),. Anal. Calcd for $C_{19}H_{19}N_3O$ (305.19): C, 74.40; H, 6.22; N 13.76; Found C, 74.23; H, 6.13; N, 13.35%.

4-(4-Thiophene)-3-methyl-1-phenyl-1*H*pyrazol-5(4*H*)-one (2b) L_2

Orange, mp = 125 °C, yield 74% IR (KBr, *ν*, cm^{-1}): 3448 (OH), 1681 (C = O), 1496 cm^{-1} (C = N) and 1056 cm^{-1}(C = S). ^{1}H NMR (DMSO-d_6, 300 MHz): δ = 2.30 (s, 3H, CH_3), 7.39 (S, 1H, = CH-Ar), 8.25 (d, 3H, Ar–H). Anal. Calcd for $C_{15}H_{12}N_2OS$ (268): C, 67.16; H, 4.47; N 10.44; S, 11.94; Found C, 67.00; H, 4.32; N, 10.21; S, 11.65%.

4-(4-methoxy benzylidene)-3-methyl-1-phenyl-1*H*pyrazol-5(4*H*)-one (2c) L_3

Orange, mp = 122 °C, yield 82% IR (KBr, *ν*, cm^{-1}): 3444 (OH), 1678 (C = O), 1508 cm^{-1} (C = N) and. ^{1}H NMR (DMSO-d_6, 300 MHz): δ = 1.91 (s, 3H, CH_3), 3.69 (s, 3H, -OCH_3), 7.20 (S, 1H, = CH-Ar), 8.71 (d, 3H, Ar–H). Anal. Calcd for $C_{18}H_{16}N_2O_2$ (292): C, 73.97; H, 5.47; N 9.58; Found C, 73.78; H, 5.13; N, 9.34%.

Synthesis of the complexes

The brown solid complex $[Ag(L_1)_2(H_2O)_2]NO_3$ was prepared by adding 0.5 mmol (0.085 g) of $AgNO_3$ in 20 ml of acetone to a stirred suspended solution 1 mmol (0.305 g) of L_1 in 50 ml acetone. The reaction mixture was refluxed for 6 h, the precipitate was drained off, washed several times with acetone and dried under vacuum over anhydrous $CaCl_2$. Dark brown $[Ag(L_2)_2(H_2O)_2]NO_3.H_2O$, $[Ag(L_3)_2(H_2O)_2]NO_3$ solid complexes were prepared in the same manner as mentioned above.

$[Ag(C_{19}H_{19}N_3O)_2(H_2O)_2]NO_3$ ($AgC_{38}H_{42}N_7O_7$) complex

Brown; Yield: 85%; m.p.: 160 °C; M.Wt: 816.65; Elemental analysis for $AgC_{38}H_{42}N_7O_7$: found, C, 55.31; H, 4.99; N, 12.00; Ag, 13.14; Calcd, C 55.89; H, 5.18; N, 12.01; Ag, 13.21; Λ_m = 115.75 S cm^2 mol^{-1}; IR (KBr, *ν*, cm^{-1}): 3450 m,br (OH), 1666 m (C = O), 1523vw cm^{-1}(C = N) and 813w and 837w (M–N). ^{1}H NMR (DMSO-d_6, 300 MHz): δ = 2.49 (s, 3H, CH_3), 3.46 (s, 2H, H_2O), 2.27–2.33 (s, 6H, -N $(CH_3)_2$), 9.67 (S, 1H, = CH-Ar), 7.14–7.97 (m, 4H, Ar–H).

$[Ag(C_{15}H_{12}N_2OS)_2(H_2O)_2]NO_3.H_2O$ ($AgC_{30}H_{30}N_5O_8S_2$) complex

Dark brown; Yield: 74%; m.p.: 125 °C; M.Wt: 760.59; Elemental analysis for $AgC_{30}H_{30}N_5O_8S_2$: found, C, 47.22; H, 3.91; N, 9.15; Ag, 14.13; Calcd, C, 47.37; H, 3.98; N, 9.21; Ag, 14.18; Λ_m = 135.50 S cm^2 mol^{-1}; IR (KBr, *ν*, cm^{-1}): 3444 m, br (OH), 1685 m (C = O), 1527vw cm^{-1} (C = N), 1099 m cm^{-1}(C = S), 748w and 792w (M–N). ^{1}H NMR (DMSO-d_6, 300 MHz): δ = 2.49 (s, 3H, CH_3), 3.37 (s, 2H, H_2O), 8.64 (S, 1H, = CH-Ar), 7.20–7.94 (d, 3H, Ar–H).

$[Ag(C_{18}H_{16}N_2O_2)_2(H_2O)_2]NO_3$ ($AgC_{36}H_{36}N_5O_9$) complex

Dark brown; Yield: 90%; m.p.: 150 °C; M.Wt: 790.57; Elemental analysis for $AgC_{36}H_{36}N_5O_9$: found, C, 54.47; H, 4.11; N, 8.80; Ag, 13.60; Calcd, C, 54.69; H, 4.59; N, 8.86; Ag, 13.64; Λ_m = 114.52 S cm^2 mol^{-1}; IR (KBr, *ν*, cm^{-1}): 3444 (OH), 1678 (C = O), 1520 cm^{-1} (C = N), 759w and 779w (M–N). ^{1}H NMR (DMSO-d_6, 300 MHz): δ = 2.33 (s, 3H, CH_3), 3.31 (s, 3H, -OCH_3), 8.42 (S, 1H, = CH-Ar), 7.18–7.46 (d, 3H, Ar–H).

Supplementary information

Supplementary information accompanies this paper at https://doi.org/10.1186/s13065-020-00723-0.

Additional file 1: Table S1. UV-Vis. spectral data of the free ligand L_1, L_2, L_3 and their Ag(I)-complexes. **Table S2.** Selected ^{1}H NMR data of L_1, L_2, L_3 and its diamagnetic complexes. **Fig. S1.** TGA and DTG diagrams for **a** L_1, **b** $[Ag(L_1)_2(H_2O)_2]NO_3$, **c**, L_2 **d** $[Ag(L_2)_2(H_2O)_2]NO_3.H_2O$, **e** L_3 and **f** $[Ag(L_3)_2(H_2O)_2]NO_3$. **Fig. S2.** The diagrams of kinetic parameters of L_1, $[Ag(L_1)_2(H_2O)_2]NO_3$, L_2, $[Ag(L_2)_2(H_2O)_2]NO_3.H_2O$, L_3 and $[Ag(L_3)_2(H_2O)_2]$ NO_3using Coats-Redfern (CR) and Horowitz-Metzger (HM) equations. **Scheme S1.** Fragmentation pattern of $[Ag(L_1)_2(H_2O)_2]NO_3$. **Scheme S2**. Fragmentation pattern of $[Ag(L_2)_2(H_2O)_2]NO_3.H_2O$. **Scheme S3.** Fragmentation pattern of $[Ag(L_3)_2(H_2O)_2]NO_3$

Abbreviations

EtOH: Ethanol; NMR: Nuclear magnetic resonance; IR: Infrared radiation; DMSO: Dimethyl sulfoxide; MIC: Minimum inhibation concentrations.

Acknowledgements

The authors gratefully acknowledge to Zagazig University (http://www.zu.edu.eg/), Egypt, Univeristy of Bisha, Saudi Arabia and Center for Advanced Materials, Qatar University, Doha, for the support of this research work.

Authors' contributions

WSS and WHE carried the literature and designed synthetic schemes (synthesis and Purifcation) and records the ^{13}CNMR of all compounds. SFM, AMA, MHS and WHE designed the research study and wrote the manuscript. WHE carried out the spectroscopic analysis and carried out the antimicrobial assays. WSS and WHE discussed the results and revised the manuscript. All authors read and approved the fnal manuscript.

Funding

This research is not funded though any source to This publication was supported by Qatar University, internal grant number QUCG-CAM-20/21-2. The findings achieved herein are solely the responsibility of the authors.

Availability of data and materials

The datasets used and/or analysed during the current study available from the corresponding author on reasonable request.

Ethics approval and consent to participate

Not applicable.

Consent for publication

All authors consent to publication.

Competing interests

The authors declare that they have no competing interests.

Author details

[1] Department of Chemistry, Faculty of Science, Zagazig University, Zagazig 44519, Egypt. [2] Center for Advanced Materials, Qatar University, P.O. Box 2713, Doha, Qatar. [3] Department of Chemistry, College of Science, University of Bisha, Bisha 61922, Saudi Arabia.

Received: 14 August 2020 Accepted: 27 November 2020
Published online: 05 December 2020

References:

1. Daniele C, Alessandro DL, Marco R et al (2008) Synthesis, biological evaluation and SAR study of novel pyrazole analogues as inhibitors of Mycobacterium tuberculosis. Bioorg Med Chem 16(18):8587–8591
2. Castagnolo DMF, Radi M, Bechi B et al (2009) Synthesis, biological evaluation, and SAR study of novel pyrazole analogues as inhibitors of Mycobacterium tuberculosis: part 2. Synthesis of rigid pyrazolones. Bioorg Med Chem 17(15):5716–5721
3. Anshu D, Ruby S, Dharmendra S et al (2010) Regioselective Synthesis of Diltiazem Analogue Pyrazolo[4,3-c][1,5]benzothiazepines and Antifungal Activity. Phosphorus Sulfur Silicon Relat Elem 185(12):2472–2479
4. Sureshkumar EV, Rao RM et al (2012) Synthesis, characterization and biological evaluation of novel pyrazole ring contain mannich derivatives. Der Pharma Chemica 4(2):707–713
5. Ouyang G, Chen Z, Cai XJ, Song BA et al (2008) Synthesis and antiviral activity of novel pyrazole derivatives containing oxime esters group. Bioorg Med Chem 16(22):9699–9707
6. Idrees GA, Aly OM, Abuo-Rahma GEAA et al (2009) Design, synthesis and hypolipidemic activity of novel 2-(naphthalen-2-yloxy)propionic acid derivatives as desmethyl fibrate analogs. Eur J Med Chem 44(10):3973–3980
7. Hu Y, Wei P, Zhou H et al (2006) Organic synthesis in ionic liquids: condensation of 3-Methyl-1-phenyl-5-pyrazolone with carbonyl compounds catalyzed by ethylenediammonium diacetate (EDDA). Chin Chem Lett 17:299–301
8. Umesha KB, Rai KML, Nayaka MAH (2009) Antioxidant and Antimicrobial Activity of 5-methyl-2-(5-methyl-1, 3-diphenyl-1H-pyrazole-4-carbonyl)-2, 4-dihydro-pyrazol-3-one. Inter J Biomed Sci 5(4):359
9. Dongmei L, Liping S, Shaodi S et al (2007) Regioselective synthesis of 6-trifluoromethyl-1,4,5,6-tetrahydropyrazolo[3,4-b]pyran derivatives. J Fluorine Chem 128(8):952–957
10. Xiao-Liu L, Yong-Mei W, Bing T et al (1998) The solid-state michael addition of 3-methyl-1-phenyl-5-pyrazolone. J Heterocycl Chem 35(1):129–134
11. Mohd A, Shikha K (2005) Synthesis and anti-inflammatory, analgesic, ulcerogenic and lipid peroxidation activities of 3,5-dimethyl pyrazoles, 3-methylpyrazol-5-ones and 3,5-disubstituted pyrazolines, Indian. J Chem 44B:2532–2537
12. Vijesh AM, Arun MI, Shrikrishna I et al (2011) Synthesis of some new pyrazolone derivatives as potent antimicrobial agents. Der Pharma Chemica 3(4):454–463
13. Mohamed A, Gamal EAA, Alaa AH (2009) Synthesis of novel pyrazole derivatives and evaluation of their antidepressant and anticonvulsant activities. Eur J Med Chem 44(9):3480–3487
14. Mahindra TM, Rajesh TK, Vithal MK et al (2004) De novo design and synthesis of HIV-1 integrase inhibitors. Bioorg Med Chem 12(9):2317–2333
15. Das N, Verma A, Shrivastava PK (2008) Synthesis and biological evaluation of some new aryl pyrazol-3-one derivatives as potential hypoglycemic agents. Indian J Chem 47B(10):1555–1558
16. Manojkumar P, Ravi TK (2009) Subbuchettiar, G. Synthesis of coumarin heterocyclic derivatives with antioxidant activity and in vitro cytotoxic activity against tumour cells. Acta Pharm 59:159–170
17. Rishikesh VA, Cendilkumar A, Gurubasavrajswamy PM et al (2011) Pyrazolone part 3: Antibacterial activity of novel 4-substituted pyrazolone derivatives. Der Pharma Chemica 3(5):7–12
18. Bondock S, Rabie R, Etman HA, Fadda AA (2008) Synthesis and antimicrobial activity of some new heterocycles incorporating antipyrine moiety. Eur J Med Chem 43(10):2122–2129
19. Rostom SAF, El-Ashmawy IM, Abd El Razik HA et al (2009) Design and synthesis of some thiazolyl and thiadiazolyl derivatives of antipyrine as potential non-acidic anti-inflammatory, analgesic and antimicrobial agents. Bioorg Med Chem 17:882–895
20. Kucukguzel SG, Rollas S, Erdeniz H et al (2000) Synthesis, characterization and pharmacological properties of some 4-arylhydrazono-2-pyrazoline-5-one derivatives obtained from heterocyclic amines. Eur J Med Chem 35(7–8):761–771
21. Meng L, Bao-Xiang Z (2014) Progress of the synthesis of condensed pyrazole derivatives (from 2010 to mid-2013). Eur J Med Chem 85:311–340
22. Douglass FT, Pavan KT (2011) Indole synthesis: a review and proposed classification. Tetrahedron 67:7195–7210
23. Demetrio R, Benedetta M, Maria VR (2015) Recent advanced in bioactive systems containing pyrazole fused with a five membered heterocycle. Eur J Med Chem 97:732–756
24. Frederick EB, Vara Prasad JVN, Allison LC et al (2007) Synthesis and SAR of novel conformationally-restricted oxazolidinones possessing Gram-positive and fastidious Gram-negative antibacterial activity. Part 1: substituted pyrazoles. J Bioorg Med Chem Lett. 17(16):4694–4698

25. Paul S, Jim CC, Alan H, Paul GG (2019) The variable toxicity of silver ions in cell culture media. Toxicol In Vitro 60:154–159
26. Tomislav B, Franc P, Tomislav M et al (2020) Ligand influence on the formation of exo-coordinated silver(I) complexes with N_2O_2 Schiff base macrocycles and the role of anion in supramolecular aggregation. Polyhedron 190:114774
27. Mann FG, Saunders BC (1960) In practical organic chemistry, 4th edn. New Impression, Orient Longman Ltd., New Delhi, p 271
28. Salem AB (2008) Thermal condensation of 1-Aryl/ hetaryl-3-methyl-2-pyrazolin-5-ones with Aromatic Aldehydes. Synthesis of 4-arylidenepyrazolones. JKAU 20(2):93–100
29. Singh V, Katiyar A, Singh S (2008) Synthesis, characterization of some transition metal (II) complexes of acetone p-amino acetophenone salicyloyl hydrazone and their anti microbial activity. Biometals 21(4):491–501
30. El-Shwiniy WH, Shehab WS, Zordok WA (2020) Spectral, thermal, DFT calculations, anticancer and antimicrobial studies for bivalent manganese complexes of pyrano[2,3-d]pyrimidine derivatives. J Mol Struct 1199:126993
31. Shehab WS, El-Shwiniy WH (2018) Nanoparticles of manganese oxides as efcient catalyst for the synthesis of pyrano[2,3-d]pyrimidine derivatives and their complexes as potent protease inhibitors. J Iran Chem Soc 15:431
32. El-Megharbel SM, Hamza RZ, Refat MS (2014) Synthesis, chemical identification, antioxidant capacities and immunological evaluation studies of a novel silver(I) carbocysteine complex. Chem-Biol Interact 220:169
33. Abo-Aly MM, Salem AM, Sayed MA et al (2015) Spectroscopic and structural studies of the Schiff base 3-methoxy-N-salicylidene-o-amino phenol complexes with some Transition metal ions and their antibacterial, antifungal. Spectrochim Acta A 136:993–1000
34. Khalil SME, Seleem HS, Shetary BA et al (2002) Mono- and Bi-nuclear metal complexes of schiff-base hydrazone (ONN) derived from o-hydroxyacetophenone and 2-amino-4-hydrazino-6-methyl pyrimidine. J Coord Chem 55(8):883–899
35. Bin H, Gang W, Wei Y et al (2011) Azo-hydrazone tautomerism by in situ CuII ion catalysis and complexation with the H2O2 oxidant of C.I. Disperse Yellow 79. Dyes Pigm. 91(2):105
36. Sultana N, Arayne MS, Gul S et al (2010) Sparfloxacin–metal complexes as antifungal agents—their synthesis, characterization and antimicrobial activities. J Mol Struct 975:285
37. Sadeek SA, Refat MS, Hashem HA (2006) Complexation and thermogravimetric investigation on tin(II) and tin(IV) with norfloxacin as antibacterial agent. J Coord Chem 59:759–775
38. Skauge T, Turel I, Sletten E (2002) Interaction between ciprofloxacin and DNA mediated by Mg^{2+}-ions. Inorg Chem Acta 339:239–247
39. Coats AW, Redfern JP (1964) Kinetic parameters from thermogravimetric data. Nature 201:68–69
40. Horowitz HW, Metzger G (1963) A new analysis of thermogravimetric traces. Anal Chem 35:1464
41. Sestak J, Satava V, Wendlandt WW (1973) The study of heterogeneous processes by thermal analysis. Thermochim Acta 7(5):333–334
42. El-Shwiniy WH, Shehab WS, Mohamed SF, Ibrahium HG (2018) Synthesis and cytotoxic evaluation of some substituted pyrazole zirconium (IV) complexes and their biological assay. Appl Organometal Chem 32:e4503
43. Elshwiniy WH, Asmaa GI, Sadeek AS et al (2020) Ligational, density functional theory, and biological studies on some new Schiff base 2-(2-hydroxyphenylimine)benzoic acid (L) metal complexes. Appl Organomet Chem 34:e5819
44. Okulik N, Jubert AH (2005) Theoretical analysis of the reactive sites of non-steroidal anti-inflammatory drugs. Internet Electron J Mol Des 4:17
45. Zaky RR, Yousef TA (2011) Spectral, magnetic, thermal, molecular modelling, ESR studies and antimicrobial activity of (E)-3-(2-(2-hydroxybenzylidene) hydrazinyl)-3-oxo-n (thiazole-2-yl) propanamide. J Mol Str 1002:76
46. Mohamed GG, Sharaby CM (2007) Metal complexes of Schiff base derived from sulphametrole and o-vanilin Synthesis, spectral, thermal characterization and biological activity. Spectrochim Acta A 66:949
47. Efthimiadou EK, Katsaros N, Karaliota A et al (2007) Synthesis, characterization, antibacterial activity, and interaction with DNA of the vanadyl-enrofloxacin complex. Bioorg Med Chem Lett 17:1238–1242
48. Dharmaraj N, Viswanathamurthi P, Natarajan K (2001) Ruthenium(II) complexes containing bidentate Schiff bases and their antifungal activity. Transit Met Chem 26:105–109

Publisher's Note